JOURNAL OF CATALYSIS 107, 375–392 (1987)

Structure of Catalytic Sites on Hydrogen-Treated Copper-Containing Spinel Catalysts

L. JALOWIECKI, G. WROBEL, M. DAAGE,[1] J. P. BONNELLE

Laboratoire de catalyse heterogene et homogene, U. A. CNRS n° 402, Universite des sciences et techniques de Lille, 59655 Villeneuve d'Ascq, France

Received June 24, 1986; revised April 22, 1987

This is a comparative study of the catalytic properties of copper chromites and copper aluminate. The purpose of this study is to identify the nature of the active sites. An analysis of the catalytic properties of various copper-containing catalysts demonstrates the critical importance of the octahedral environment of cuprous ions. Hydride ions, located in anionic vacancies (BMV) shared between the cuprous ion and the chromium or aluminium ion, are the primary active species. The second cation (Cr^{3+}, Al^{3+}) is primarily a stabilizer of a defect spinel oxide phase. Since hydrogen reservoir capacity plays an important role in the hydrogenation of dienes, the variation of the occluded hydrogen concentration was studied as a function of the calcination temperature of the oxide precursor as well as a function of the second cation. Taking into account the spinel unit cell, structures of the catalytic sites are proposed. These structures are consistent with the well-known synergism in copper-containing catalysts.

INTRODUCTION

For many years, copper-containing catalysts were extensively used in industrial processes, such as selective hydrogenation of vegetable oils, fragrance synthesis, and methanol synthesis (*1–7*). Although numerous authors agree on the catalytic importance of cuprous ions, some controversy still exists on the nature of the active species (*7–9*). In our previous work on bulk copper chromites, we reported a direct correlation among the activity of the catalyst, the concentration of cuprous ions in an octahedral environment, and the concentration of occluded hydrogen (*9, 10*). A nucleophilic attack and carbanion intermediates were used to describe the variation in selectivity for the hydrogenation of dienes (*11*). The formation of copper hydride species is consistent with all the mechanistic results. Similar species were also proposed in homogeneous catalysis (*12*).

This article presents a comparative analysis of $Cu_2(II)Cr_2O_x$, $Cu(I)Cr_2O_x$, and $Cu(II)Al_2O_4$ and reports on the structure of the catalytic sites, consistent with the synergism observed in such systems. We focused our attention on the relationship among the environment of the cuprous ion, the role of the second cation, the catalytic activity, and the hydrogen storage capabilities of bulk materials.

EXPERIMENTAL

Samples

The various samples of copper chromium oxides (Cu/Cr = 0.5 or 1.0) were prepared by coprecipitation of copper and chromium hydroxides with ammonium hydroxide. The oxide precursors were obtained by thermal decomposition under flowing nitrogen at temperatures ranging from 370 to 650°C for the various cupric chromites and 800°C for the cuprous chromite, according to the procedure already described (*13*). The cupric chromite precursors were then reduced at 150°C with flowing hydrogen. The cuprous chromite was used as is.

[1] To whom all correspondence should be addressed at Exxon Research and Engineering Co., Route 22 East, Annandale, NJ 08801.

0021-9517/87 $3.00

The copper aluminium oxide was also prepared by coprecipitation of the corresponding hydroxides, followed by thermal decomposition under flowing air at 810°C. The reduction of the aluminate began around 150°C, and two different solids were obtained, as shown by the TGA analysis (Fig. 1). Between 150 and 300°C, the formation of metallic copper particles on a residual spinel was observed by X-ray diffraction. Above 350°C complete segregation occurred, and metallic copper supported on γ-alumina was observed by X-ray. The cupric aluminate was reduced at 300°C before the catalytic run. Finally, the specific areas of all the catalysts were measured by the BET method.

All the gases (Air liquide, U-grade, >99.9%), as well as the hydrocarbons (Fluka, puriss grade, >99.5%), were used after further purification.

Procedure and Apparatus

Thermogravimetric analysis. The TGA experiments were carried out on a Sartorius 4102 microbalance, equipped with a gas flow system, previously described (*14*). One hundred milligrams of oxide precursor was loaded into a quartz basket and dried with a flow of purified nitrogen. This state was used as a mass reference. The solid was then reduced with hydrogen (10% in nitrogen) by increasing the temperature from 25 to 400°C at a rate of 1°C/min.

Catalytic activity measurement. The catalytic measurements were carried out in an all-glass, grease-free flow unit, previously described in the literature (*15*) (Fig. 2). The diene was introduced at constant pressure (20 Torr) by distillation in a subambient trap (−50°C) and swept away with a flow of dried purified hydrogen, deuterium, or helium (20–60 ml/min, atmospheric pressure). Fifty to one hundred fifty milligrams of catalyst was loaded in a pulsed isothermal microreactor, operating at temperature ranging from 40 to 350°C, depending on the catalyst treatment. Variations in conversion levels were achieved by changing either the reaction temperature or the flow rate of the carrier gas.

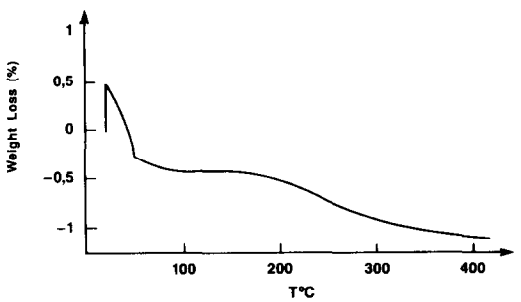

FIG. 1. Cuprous chromite TGA in the presence of hydrogen.

Occluded hydrogen measurement by isoprene hydrogenation. After reduction of the oxide precursor, the catalyst was flushed with purified dry helium (60 ml/min) for 20 min. The elimination of gaseous hydrogen was confirmed using both a conductivity cell inserted in the gas flow line and GC analysis. After 10 min, the hydrogen concentration was less 0.1%. Then 5 Torr of isoprene was introduced into the helium flow line. The isoprene hydrogenation was monitored by GC analysis. When the hydrogenation was completed, the total amount of occluded hydrogen was estimated by integrating the total concentration of all pentenes versus time. This total hydrogen amount will be referenced as H* in the text.

In order to confirm that all hydrogen was eliminated from the flow system, a control experiment was performed. A 10% platinum on alumina catalyst was substituted for the copper catalyst. This catalyst showed negligible hydrogen storage capacity even though it has a high hydrogenation activity in the presence of gaseous hydrogen. This negligible total hydrogenation clearly demonstrates that the hydrogen had been eliminated from the gas flow line.

Occluded hydrogen measurement by deuteration. After reduction of the oxide precursor, the hydrogen flow was switched to a deuterium gas flow for 20 min. The elimination of gaseous hydrogen was con-

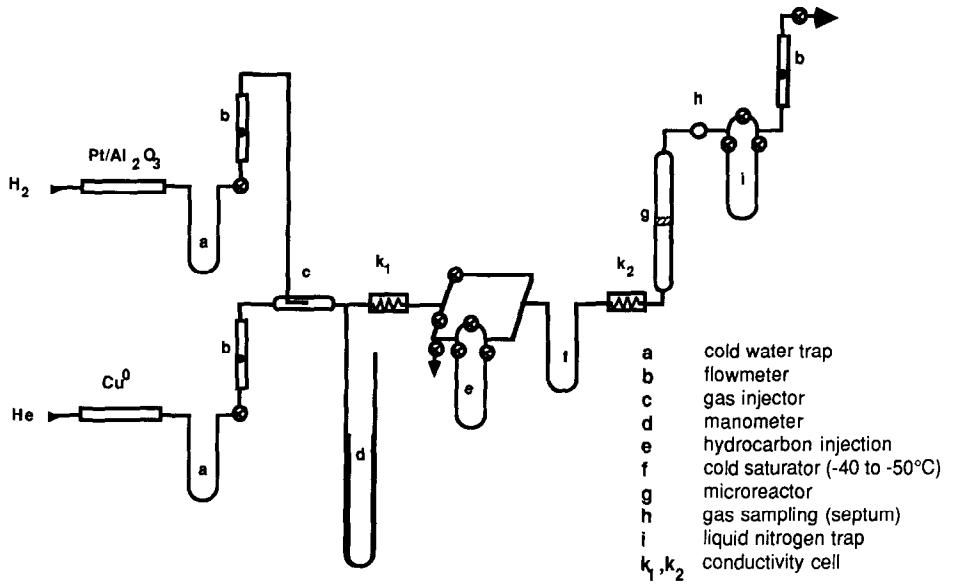

FIG. 2. Catalytic reactor.

firmed by mass spectrometry and residual concentration was lower than 0.1%. Then 5 Torr of isoprene was added to the helium flow, and the products were collected in five to seven fractions of 20–30 μl. The deuterium content of these various fractions was determined by mass spectrometry. The total occluded hydrogen was then estimated by the difference between the number of deuterium atoms introduced in the products and the stoichiometry of the reaction (two deuterium atoms per pentene molecule).

Note that the consistency between the hydrogen consumption and the deuteration method provides further clear evidence that the gaseous hydrogen was eliminated from the gas flow line.

Product Analysis

The product distribution was determined by GC, using a Varian 3700 chromatograph, equipped with a flame ionization detector and a capillary column (squalane, 0.2 mm i.d., 100 m long) operating at 40°C.

In tracer experiments, the deuterium content of the various products was determined by mass spectrometry, using the method described by Gault and Kemball (*16*). Parent peaks were used after the usual corrections for natural isotope. The fragmentation corrections for the various deutero molecules were made on a statistical basis, using the fragmentation patterns of nonlabeled and perdeuterated molecules. The C–D fragmentation in the C_5 hydrocarbons was 0.77 of that of C–H bond, i.e., identical to the isotopic effect observed in butenes (*17*). The mass spectra were recorded on a Ribermag R10-10-Sydar mass spectrometer.

RESULTS

Catalytic Activity and Selectivity

The hydrogenation activity was measured at 50°C, using isoprene as a model compound. Because the various catalysts were prepared at different temperatures, large variations in specific areas were obtained. Therefore, the hydrogenation activities are reported per gram of catalyst as well as per square meter (Table 1). Both cupric chromite (CuCr-1) and cupric aluminate exhibited a similar activity per square meter. However, a lower activity was obtained for the cupric chromite catalysts whose Cu/Cr ratio is 0.5 and decreased as a

TABLE 1

Catalyst	Cu/*M*	Temperature (°C)			BET (m^2/g)	Hydrogenation activity	
		Annealing	Reduction	Reaction		(per g)	(per m^2)
Cupric chromite							
CuCr-0.5	0.5	370	150	50	64.4	16.55	0.26
CuCr-0.5*	0.5	500	150	50	21.4	3.58	0.17
CuCr-0.5**	0.5	650	150	50	8	0.56	0.07
CuCr-1	1.0	370	150	50	77	33.11	0.43
Cupric aluminate							
CuAl-0.5	0.5	800	300	50	7	3.15	0.45
Cuprous chromite	1.0	800	200	200	1	0.1 ($\sim 10^{-4}$)[a]	<0.1 ($\sim 10^{-4}$)[a]

[a] The values in brackets are calculated activities at 50°C, using an activation energy of 54 kJ/mole.

function of the calcination temperature. The direct correlation between the hydrogenation activity and the concentration of the Cu(I) ions (*9*) suggests that the concentration of cuprous ions per surface unit is lower for the catalysts treated at high temperatures. The relatively high activity per square meter of the aluminate was surprising considering the high temperature used for its synthesis.

By contrast, the cuprous chromite was found to be inactive at 50°C; a significant activity was observed only at temperatures higher than 200°C. As shown by the TGA analysis in hydrogen atmosphere, a continuous weight loss was observed above 200°C (Fig. 3). In this temperature range, X-ray diffraction showed that the cuprous chromite phase collapsed and that metallic copper supported on chromia is formed. Consequently, the behavior of the cuprous chromite appeared very similar to the behavior of the cuprous oxide and bulk metallic copper catalysts, as reported in the literature (*18, 19*). Finally, it is noteworthy that the cupric chromite Cu/Cr = 1 was the most active catalyst because of its low temperature synthesis that led to a high surface area, and because of its ionic distribution.

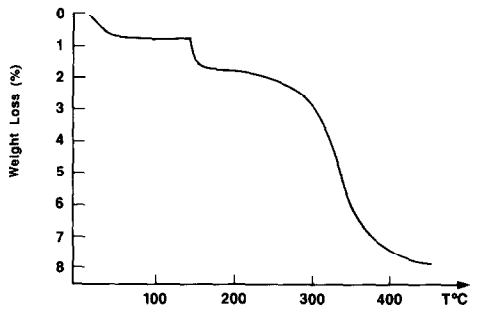

FIG. 3. Cupric aluminate TGA in the presence of hydrogen.

Typical variations in the product distribution with the conversion level are represented in Figs. 4 and 5. For the isoprene hydrogenation, the 2-methyl-1-butene and the 3-methyl-1-butene corresponded to primary products while the 2-methyl-2-butene was a secondary product. By contrast, all of the pentenes resulted from the primary hydrogenation of the *trans*-1,3-pentadiene. In Tables 2 and 3, the selectivities of the various catalysts are compared. The 1-pentene and the 2-methyl-1-butene were always the major components. With the exception of cuprous chromite, all the catalysts exhibited a very similar selectivity, independent of the type of catalyst used, as observed previously (*20*). Therefore, the significant difference observed for

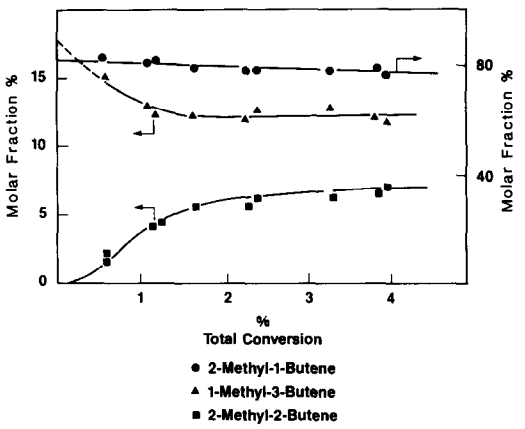

FIG. 4. Isoprene hydrogenation on cupric chromite (CuCr-1). Typical product distribution.

the cuprous chromite is attributed to the high reaction temperature used, rather than to the nature of the catalyst itself.

The apparent activation energies for the various hydrogenation reactions of the isoprene and the *trans*-1,3-pentadiene are reported in Table 4 for the Cu/Cr = 1 chromite and the aluminate. In general, these values were lower than those observed on metallic copper or supported catalysts: 56.4 and 54.3 kJ/mole, respectively (*18, 21*).

Measurement of the Occluded Hydrogen Amount

By isoprene hydrogenation. In the previous studies, we reported that the cupric

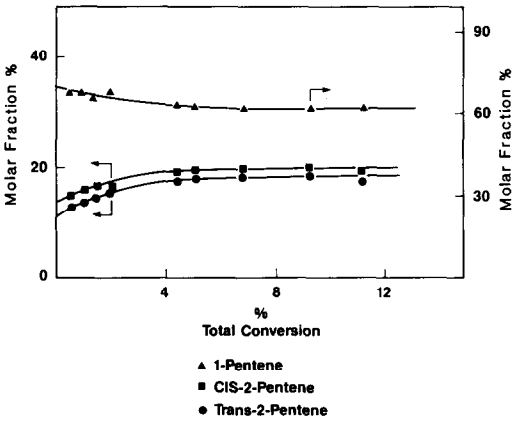

FIG. 5. *trans*-1,3-Pentadiene hydrogenation on cupric chromite (CuCr-1). Typical product distribution.

TABLE 2

Selectivity in the Isoprene Hydrogenation

Catalyst	3-Methyl-1-butene (%)	2-Methyl-1-butene (%)	2-Methyl-2-butene (%)
CuCr-1	12	79	7
CuCr-0.5	10	82	8
CuCr-0.5*	11	80	9
CuAl-0.5	10	83	7
Cuprous chromite[a]	21	62	17

[a] Catalytic hydrogenation carried out 220°C.

chromite (Cu/Cr = 1) behaved like a reversible hydrogen reservoir, whose content can be precisely controlled (*22, 23*). At 150°C, isoprene (5 Torr in helium) can be hydrogenated by the hydrogen species occluded in the bulk of the catalyst. As shown in Fig. 6, a continuous decrease in the relative hydrogenation rate occurred and led to a total extraction of the occluded hydrogen. By integration of the rate versus time curves, the total amount of extractible hydrogen (H*) was estimated and corresponded to 4.7 ± 0.5 and 0.66 ± 0.03 μmole/g for the cupric chromite (Cu/Cr = 1) and the cupric aluminate. The lower content, found for the aluminate, might be related to the nature of the catalyst itself or to its high temperature synthesis. Since the hydrogenation rates changed in a different manner, different mechanisms for the hydrogen extraction might be involved (Fig. 6). For the cupric chromite, the mechanism previously proposed corresponds to the diffusion of the hydrogen species from the bulk to the surface, followed by the regen-

TABLE 3

Selectivity in the *trans*-1,3-Pentadiene Hydrogenation

Catalyst	1-Pentene (%)	*cis*-2-Pentene (%)	*trans*-2-Pentene (%)
CuCr-1	63	17	20
CuCr-0.5	68.6	15	16.4
CuCr-0.5*	65	18.2	16.8
CuAl-0.5	65.5	13.5	21

TABLE 4

Apparent Activation Energies (kJ/Mole)

Catalyst	Reactant	Hydrogenation			*cis–trans* Isomerization
		1-Pentene or 2-methyl-1-butene	*t*-2-Pentene or 3-methyl-1-butene	c-2-Pentene or 2-methyl-2-butene	
CuCr-1	*t*-1,3-Pentadiene	41.0	45.1	43.5	24.2
	Isoprene	35.5	42.6	62.7	
CuAl-0.5	*t*-1,3-Pentadiene	33.4	50.2	48.1	20.9
	Isoprene	29.3	46.0	58.5	

eration of the hydrogenation site (*23*). The surface remained hydrogen saturated as long as enough hydrogen was provided by the bulk. The rate-limiting step is then the regeneration of the hydrogenation site, according to the sequence

$$H_B \rightarrow H_S$$ rapid diffusion from the bulk to the surface

$$S + H_S \xrightarrow{K} S\text{-}H_S$$ hydrogenation site regeneration

$$S\text{-}H_S + \text{diene} \xrightarrow{k} R\text{—}\overset{H}{\underset{}{\diagup}}\underset{S}{\diagdown}$$ hydrogenation reaction,

where H_B, H_S are the hydrogen species in the bulk and on the surface and S is the catalytic site on which the hydrogenation occurs. The hydrogenation extraction is then described by the set of equations

$$\frac{V_t}{V_0} = \frac{K/kH_S^0 + e^{-kt(1+K/kH_S^0)}}{1 + K/kH_S^0} \quad \text{when } H_B \neq 0$$

and

$$\frac{V_t}{V_0} = \frac{K/kH_S}{1 + K/kH_S} \quad \text{when } H_B = 0,$$

where V_0 and V_t are the hydrogenation rates at times 0 and t, H_S^0 and H_S are the hydrogen concentrations on the surface at times 0 and t, and K and k are the rate constants for the regeneration of the site and the hydrogenation reaction.

As shown in Fig. 7, the behavior of the cupric aluminate and the cupric chromite can be fit with the same set of equations, suggesting that the mechanism is valid for both catalysts. The values of the various parameters, compiled in Table 5 correspond to the best fits. The rate constants were slightly higher for the cupric alumi-

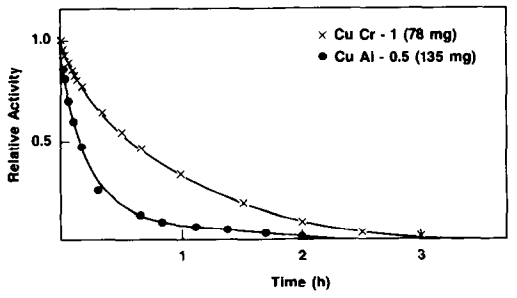

FIG. 6. Consumption of the occluded hydrogen versus time.

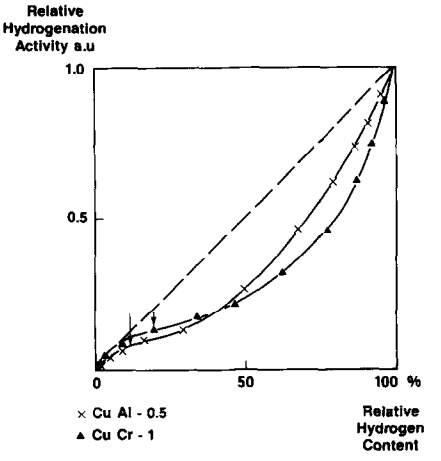

FIG. 7. Comparison of the hydrogenation rates versus the hydrogen content of the solid.

TABLE 5

Optimized Parameters for the Hydrogen Extraction of the Cupric Chromite and Cupric Aluminate

	CuCr-1	CuAl-0.5
$[H_S^0]/[H_B^0]$	0.18	0.11
k (min^{-1})	0.067	0.095
K/k	0.70	0.75
$k/k[H_S^0]$	0.14	0.12

nate whereas more hydrogen was located on the surface of the cupric chromite.

By deuteration of isoprene. The deuteration of isoprene was carried out under a deuterium gas flow on catalysts previously reduced with gaseous hydrogen. The reaction conditions (temperature, gas flow rate, hydrocarbon pressure) were strictly identical to those used for the catalytic reaction

TABLE 6

Isotopic Distribution in the Reaction Products for the Cupric Chromite

Charge No.		1	2	3	5	7
3-Methyl-1-butene	α_i%	1.3	1.3	1.3	1.3	1.2
	d_0	57.8	47.0	45.9	46.7	52.2
	d_1	26.8	38.7	37.9	35.4	31.7
	d_2	13.9	11.7	12.9	14.3	11.8
	d_3	0.3	2.3	2.9	3.0	3.5
	d_4	1.2	0.4	0.4	0.7	0.7
2-Methyl-1-butene	α_i%	18.1	16.7	15.3	12.4	9.5
	d_0	46.1	45.7	41.1	33.9	20.7
	d_1	39.2	38.3	38.0	41.0	46.8
	d_2	11.7	12.2	15.3	18.3	22.9
	d_3	2.5	3.3	4.3	5.5	7.6
	d_4	0.5	0.6	1.0	1.4	2.0
2-Methyl-2-butene	α_i%	1.3	1.3	1.3	1.2	1.2
	d_0	35.9	53.9	34.8	52.4	41.6
	d_1	46.8	31.5	38.6	25.1	31.1
	d_2	16.1	11.3	20.4	15.1	18.8
	d_3	1.2	2.6	5.5	5.7	6.9
	d_4	—	0.7	0.7	1.7	1.6
Isoprene	α_i%	79.3	81.0	82.5	85.0	88.0
	d_0	94.5	89.8	91.4	88.8	90.1
	d_1	5.3	9.7	8.4	10.6	9.3
	d_2	0.2	0.5	0.3	0.6	0.6
	d_3	—	—	—	—	—
	d_4	—	—	—	—	—
Total conversion	α_T%	20.7	19.0	17.5	15.0	12.0
	n_D	0.9	0.9	1.3	1.6	1.95

TABLE 7

Isotopic Distribution in the Reaction Products for the Cupric Aluminate

Charge No.		1	2	3	4	5
3-Methyl-1-butene	α_i%	1.1	0.79	0.63	0.72	1.05
	d_0	45.0	52.5	44.7	47.9	42.0
	d_1	34.8	27.5	32.7	31.2	26.0
	d_2	12.8	11.0	14.3	12.9	9.5
	d_3	5.6	7.5	7.1	5.6	3.6
	d_4	1.8	1.4	1.2	1.7	1.9
	d_5	—	—	—	0.6	—
2-Methyl-1-butene	α_i%	10.8	7.4	6.2	5.8	6.1
	d_0	45.6	51.7	36.1	27.8	25.3
	d_1	33.0	30.2	39.5	42.6	44.5
	d_2	14.8	11.9	15.7	18.2	18.3
	d_3	6.6	4.9	6.4	7.8	8.4
	d_4	—	1.4	2.3	2.9	3.5
	d_5	—	—	—	0.7	—
2-Methyl-2-butene	α_i%	0.6	0.4	0.4	0.2	0.4
	d_0	43.9	30.8	33.7	30.8	27.9
	d_1	26.2	29.3	26.1	29.5	30.1
	d_2	19.6	21.5	20.0	20.8	21.1
	d_3	10.2	12.8	13.7	13.0	13.5
	d_4	—	5.6	6.5	4.4	7.4
	d_5	—	—	—	1.5	—
Isoprene	α_i%	86.9	91.1	92.5	93.0	92.2
	d_0	95.1	94.7	94.0	94.1	94.5
	d_1	4.4	5.0	5.7	5.5	5.1
	d_2	0.5	0.3	0.3	0.4	0.4
	d_3	—	—	—	—	—
	d_4	—	—	—	—	—
Total conversion	α_T%	12.6	8.6	7.2	7.0	7.6
	n_D	1.2	1.5	1.8	2.0	2.0

carried out in the presence of gaseous hydrogen. The isotopic content of the resulting pentenes and the isoprene was determined for the various successive samples (~30 μl each). Wide distributions were observed in the pentenes, and an exchange reaction of the isoprene led to d_1 molecules (Tables 6 and 7). For both catalysts, significant amounts of hydrogen were introduced in the pentenes. If a decrease in the d_0 percentages occurred for the last samples, a selective formation of d_2 molecules was never reached because of the scrambling induced by the exchange reactions. However, the participation of the occluded hydrogen is clearly established by the average number of deuterium introduced in the total sample. This number n_D, reported in the bottom line of Tables 6 and 7, was calculated by using the expression

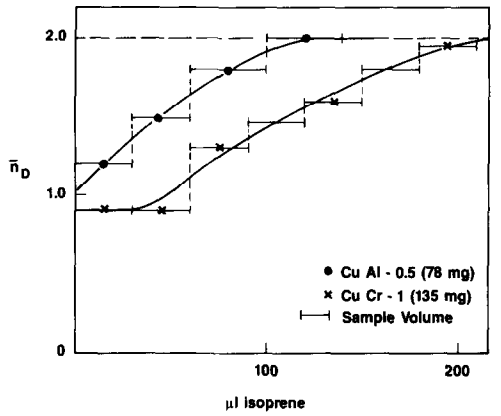

FIG. 8. Variation of $\bar{n}_D$ versus volume of isoprene injected.

$$n_D = \frac{\sum_i n_i \cdot \alpha_i}{\alpha_T} \quad \text{with } n_i = \sum_j j \cdot d_j,$$

where j is the number of deuterium in a given isotopic isomer, d_j is the molar fraction of this isotopic isomer, n_i and α_i are the average number of deuteriums in the product i and the molar fraction of product i (isoprene included), and α_T is the total conversion.

As shown in Fig. 8, these numbers continuously increased and reached the theoretical value of 2.0, when all the occluded hydrogens were substituted with deuteriums atoms. By adding the various amounts of hydrogen found in the successive samples, the total amount of exchangeable occluded hydrogen was estimated. A value of 2.8 mmole/g was found for the cupric chromite and 0.34 mmole/g for the cupric aluminate. These values were much lower than those found by the hydrocarbon extraction method and corresponded roughly to one-half (Table 8).

TABLE 8

Estimation of the Hydrogen Content

Catalyst	Hydrocarbon consumption H* (mmole/g)	Isotopic method H_D (mmole/g)	One-half of hydrogen consumption H^- (mmole/g)
CuCr-1	4.7 ± 0.5	2.8 ± 0.3	2.4 ± 0.5
CuAl-0.5	0.66 ± 0.07	0.34 ± 0.03	0.33 ± 0.07

Hydrogen Content of Various Catalysts

The hydrogen content of five different catalysts was determined by the hydrocarbon extraction method in order to study the effect of the composition and the annealing temperature on the amount of occluded hydrogen. The hydrogen content, as well as the annealing temperature, and the specific area are compiled in Table 9. The cupric chromite (Cu/Cr = 1) contained more hydrogen than any other catalyst. Its higher hydrogen content was previously attributed to its high concentration in Cu(I) in octahedral sites as well as its defect structure, compared to that of the chromite (Cu/Cr = 0.5) (9). The effect of the annealing temperature was studied on the $Cu(II)Cr_2O_4$ system because of the segregation of the (Cu/Cr = 1) catalyst at high temperatures. A sixfold decrease was observed when the temperature was increased to 650°C. Simultaneously, the specific area dropped from 64 to 8 m^2/g. As shown in Fig. 9, the variation of the hydrogen content as a function of the specific area was not linear, which is consistent with the bulk location of the hydrogen species. It is also significant to note that the cupric aluminate can potentially contain more hydrogen than its CuCrO analog, if it can be prepared at lower temperatures.

TABLE 9

Hydrogen Content of the Various Catalysts (by Hydrocarbon Consumption)

Catalyst	Annealing temperature	H* (mmole/g)	BET (m^2/g)
CuCr-1	370	4.7	77
CuCr-0.5	370	3.0	64
CuCr-0.5*	500	1.5	21
CuCr-0.5**	650	0.5	8
CuAl-0.5	800	0.7	7

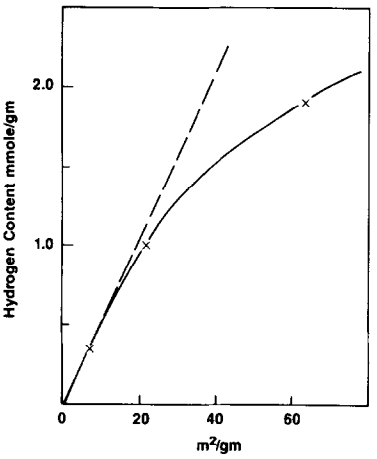

FIG. 9. Variation of the hydrogen content versus the specific area for the CuCr-0.5 catalysts.

DISCUSSION

The results of the catalytic activity measurement clearly indicated that the structure of the oxide precursor is critical. Since the hydrogenation was previously attributed to the existence of Cu(I) species in an octahedral environment (*9*), further considerations on the environment of the cupric ion in the oxide precursor and the role of the second cation (Cr(III), Al(III)) must be done.

Role of the Cu(I) Environment and of the Second Cation

Table 10 summarizes the complete formulae, proposed in the literature for the cupric chromites (*24*). For a Cu/Cr ratio of 0.5, the oxide crystallizes in a tetragonal spinel structure as previously reported by Adkins *et al.* (*25*). In contrast a cubic spinel is obtained when the Cu/Cr ratio is equal to 1 (*14*). It is noteworthy that the cupric ions exist in both tetrahedral and octahedral environments, and that their distributions depend upon the Cu/Cr ratio and the annealing temperature. The concentration of the Cu^{2+} cations in octahedral sites decreases when the Cu/Cr ratio decreases, and/or when the anneal temperature increases.

A similar structure is obtained for the cupric aluminate. However, 40% of the cupric ions is located in octahedral sites and 60% in tetrahedral sites. This distribution, determined by XPS (*26*), agrees with the values reported in the literature (*27*).

For the cupric chromites, an extensive study on the characterization was reported by Wrobel *et al.* (*28*). During the reduction, most of the cupric ions in tetrahedral sites were reduced to metallic copper, which migrates to the surface to form particles. In addition, the Cr(VI) ions, when present (Cu/Cr = 1 only), are transformed in Cr(III) species, and the Cu(II) in octahedral sites are reduced to Cu(I) ions. Moreover, a large concentration of hydroxyl groups closely attached to the chromic ions is created and some hydrogen is occluded in the solid as demonstrated by NMR (*9*). Finally, the catalyst corresponds to a biphasic system composed of metallic copper particles supported on a cubic defect spinel. Consequently, the density of Cu(I) ions in an octahedral environment appears directly related to the partial inversion of the spinel precursor. This is especially evident in the high intrinsic activity of the catalyst (Cu/Cr = 1) for which the partial inversion is maximum (Tables 10 and 1). Moreover, the intrinsic activity is dependent upon the annealing temperature as observed for the set of cupric chromites (Cu/Cr = 0.5) (Table I). In addition, this effect is related to the Cu(I) density, since a high annealing temperature results in a more crystallized solid, and a lower extent of partial inversion, as illustrated by the ionic distributions in the (Cu/Cr = 0.5) and (Cu/Cr = 0.5*) samples (Table 10).

TABLE 10

Ionic Distribution of the Cupric Chromites (*23*)

Cu/Cr	Annealing temperature	Formula[a]
0.5	370	$Cu^{2+}_{0.81}Cr^{3+}_{1.19}[Cu^{2+}_{0.15}Cr^{6+}_{0.10}Cr^{3+}_{1.63}\square_{0.12}]O^{2-}_4$
0.5	500	$Cu^{2+}_{0.90}Cr^{3+}_{0.10}[Cu^{2+}_{0.10}Cr^{3+}_{1.90}]O^{2-}_4$
1.0	370	$Cu^{2+}_{0.74}Cr^{3+}_{0.26}[Cu^{2+}_{0.58}Cr^{6+}_{0.47}Cr^{3+}_{0.59}\square_{0.36}]O^{2-}_4$

[a] The cations inside the brackets are in an octahedral environment, the other cations being in a tetrahedral environment.

For the cupric aluminate, a similar situation exists as a result of the spinel structure. However, there are some significant differences. The important partial inversion of the aluminate (40% of the copper ions in octahedral sites) results in a high density of Cu(I) active sites, and in a high intrinsic activity. The similar intrinsic activities obtained for the cupric chromite (Cu/Cr = 1) and the aluminate suggests that the turnover frequency of the Cu(I) site in the aluminate is lower. This clearly indicates that the second cation (Cr(III), Al(III) plays a significant role in the properties of the catalytic site. The higher temperature (300°C compared to 150°C for the chromites), required for the reduction of the aluminate, suggests that a more important stabilization of the copper ion in an octahedral environment occurs in the presence of the aluminum ions. This higher stabilization is also responsible for the higher partial inversion of the spinel. There are two possible explanations for the lower turnover frequency. First, the higher stabilization will decrease the ability of the site to form coordination vacancies. These coordination vacancies are generally considered to be the primary site for the adsorption of the organic molecule (*29, 30*). The higher the stabilization, the smaller the number of vacancies. Second, the reduction of the copper ions in octahedral sites to Cu(I) will be less effective when the stabilization is high. The apparent activation energy shows that the well-known synergism is more important for the aluminum ions; this supports the second explanation. Note that similar results were obtained by Berg *et al.* (*31*) and Meijden (*32*) for the CO oxidation on supported or unsupported copper oxides. The lower activation energy (33.4 kJ/mole on $CuCrO_x/SiO_2$ compared to 64 ± 1 kJ/mole on CuO and CuO/SiO_2) was attributed to the formation of particular sites where the copper and the chromium were both involved.

Finally, the cuprous chromite is an isomorph of $CuFeO_2$ and crystallizes in a rhombohedral structure, sometimes called the *delafossite* structure (*33*). The cuprous ions exist in a very distorted cubic environment, and two Cu–O bond lengths are observed: 2.05 and 3.98 Å. Therefore, a linear environment, similar to that of Cu_2O, should be considered (Scheme 1). The lack of activity of the cuprous chromite clearly shows that the quasi-linear environment of the Cu(I) ion in the delafossite structure is not adequate. This catalyst behaves like cuprous oxide (Cu_2O) which is known for its poor activity (*18*). When reduced at 200°C, cuprous chromite no longer exists. The catalyst corresponds to metallic copper on chromia and its activity is comparable to that of copper metal (*19*). These two results show that the octahedral environment of the cuprous ion is essential for the catalytic activity.

Hydrogen Storage

In a previous study, we reported that the cupric chromite (Cu/Cr = 1) behaves like a reversible hydrogen reservoir (*22, 23*). Our results clearly show that similar behavior is obtained for different Cu/Cr ratios, as well as for the cupric aluminate. However, some comments on the hydrogen extraction mechanism must be made before considering the role of the catalyst morphology on the hydrogen storage properties. The occluded hydrogen can be extracted by using two different methods: hydrogenation of isoprene in the absence of gaseous hydro-

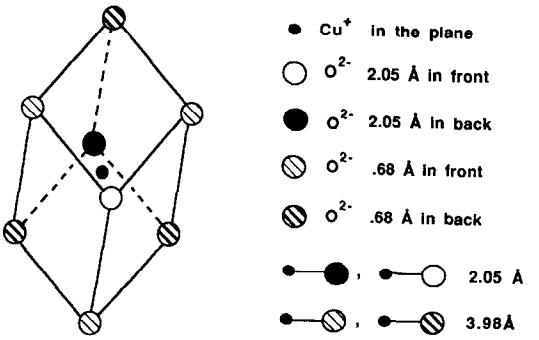

SCHEME 1. Environment of the Cu cation in the cuprous chromite.

gen, and deuteration of isoprene on a hydrogen-containing catalyst. Although these two methods result in an apparent contradiction, in terms of the amounts of occluded hydrogen, an explanation can be found in the mechanisms involved in both reactions. By using isoprene and 1,3-pentadienes as model compounds, the hydrogenation mechanism was previously described in terms of a nucleophilic attack of the diene, which leads to the formation of anionic intermediates (*11*). Consequently, a hydridic nature of the first hydrogen introduced in the molecule and a heterolytic splitting of the hydrogen were deduced. As represented in Scheme 2, the formation of the corresponding olefin can be obtained by two different routes. The first step is the addition of the hydride. Route 1, in which the proton is provided the hydroxyl groups of the catalyst, corresponds to the hydrogenation in the absence of gaseous hydrogen. Route 2 involves the regeneration of the catalytic site by the activation of molecular hydrogen or deuterium and corresponds to a hydrogenation in the presence of hydrogen or deuterium. It clearly appears that one-half of the hydrogen reservoir consists of hydride ions and that the other half is protons, provided by the hydroxyl groups. In the isotopic method, route 1 is a minor process and only the hydride concentration is measured. The proton is provided by the gas phase. This mechanism is supported strongly by the fact that initially the average number of deuterium introduced in the products is close to 1 (Fig. 8). The amount of occluded hydrogen extracted by isotopic exchange should then be roughly equal to one-half of the concentration extracted in the absence of gaseous hydrogen. From the comparison reported in Table 8, a good correlation is observed. The slightly higher value, obtained on the cupric chromite with the isotopic exchange, suggests a small participation of the hydroxyl groups, present in large concentrations in this particular catalyst.

Another interesting effect concerns the hydrogen capacity of these defect spinel phases. Our results show that the hydrogen concentration decreases significantly when the annealing temperature is increased. Therefore, the primary effect on the hydrogen storage is associated with the disorder of the material, i.e., the existence of coordination vacancies. As a result of the hydridic nature of one-half of the occluded hydrogen

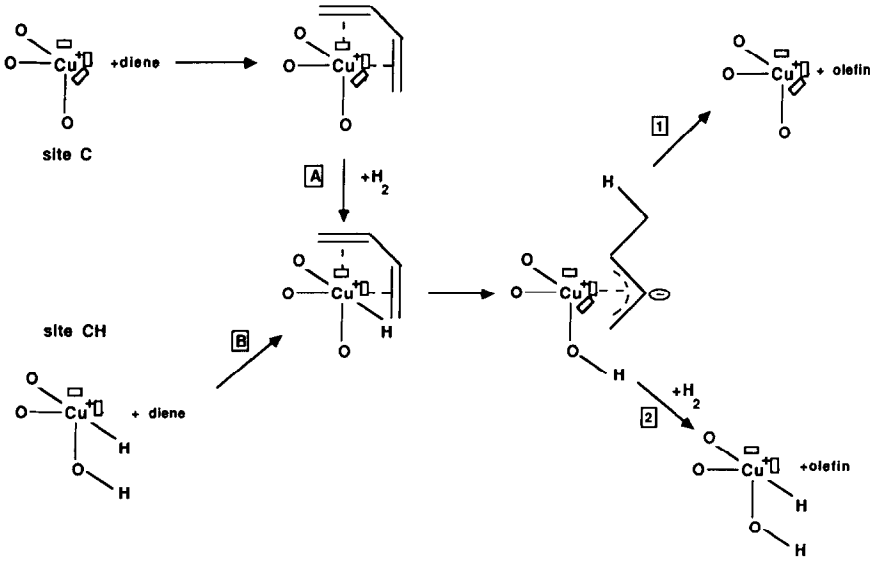

SCHEME 2. Diene hydrogenation mechanism.

species, one must assume that such hydrogen species will be located in anionic vacancies. There is further support for this assumption in the comparable size of H^-, O^-, and O^{2-} (1.54, 1.76, and 1.32 Å, respectively) (*34*). The ability to form anionic vacancies appears then to be critical for the hydrogen storage. In that sense, the cupric chromite is very particular since two different effects increase its capacity. One obviously is related to its low temperature synthesis (370°C), and the second is related to its specific area increase during the reducing treatment. In effect, the reduction of the oxide precursor leads to the formation of metallic copper particles on the surface, by extracting most of the tetrahedral cupric ions, which increases the disorder and the number of ionic vacancies. In contrast, significant amounts of the tetrahedral sites in the aluminate are occupied by aluminum ions, which cannot be extracted. Consequently no significant increase in the disorder can be obtained by the reduction. This points out another important role of the second cation, consisting in the stabilization of the defect spinel phase: the more defects, the more hydrogen storage.

Structures of the Catalytic Sites in the Defect Spinel Phase

Because the reduction of the oxide percursor leads to the formation of fairly crystalline phases, the defect spinel phase provides a good model to improve our understanding of the structure of the catalytic sites and the synergism. In the literature, the catalytic activity of numerous oxides or mixed oxides is generally associated with the existence of coordination vacancies surrounding the metallic ion (*29, 30*). By analogy with some homogeneous transition metal complexes, six different structures were proposed by Siegel (Scheme 3) (*30*). Such structures can be characterized by the reactions they induced. For example, C and CH sites were found to be specific for hydrogenation reactions. For the copper chromite, the hydrogenation is related to the cuprous species and is consistent with this model (Scheme 2) (*9, 10*). However, a rapid observation of the spinel structure clearly indicates that isolated octahedral sites are unlikely, and that the C and CH structures give a poor description of the catalyst surface by neglecting the cationic nearest neighbors (Cr(III), Al(III),

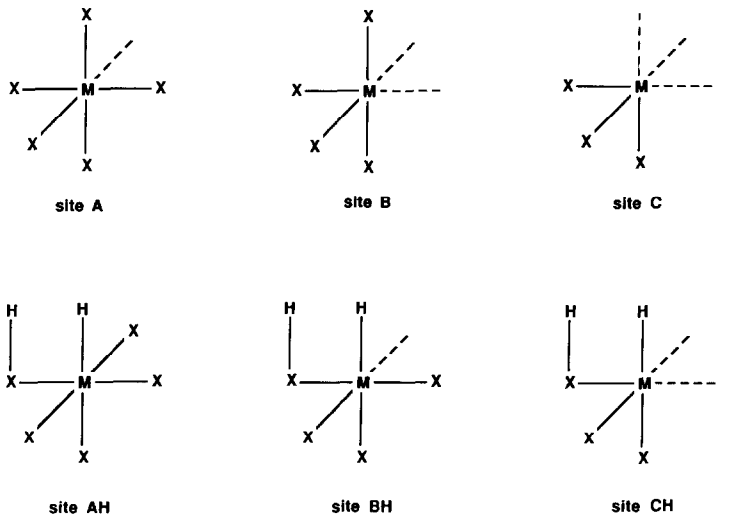

SCHEME 3. Structures of catalytic sites (*29*).

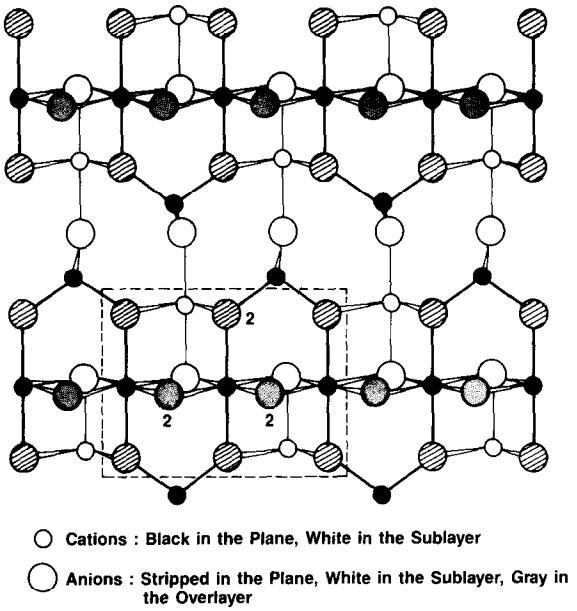

SCHEME 4. Environment of octahedral cations in the (110) plane.

Cu(I)). A surface differential neutron diffraction study by Beaufils and Barbaux (*35, 36*), has shown that the (111) and (110) planes for Co_3O_4 and the (110) and (100) planes for $MgAl_2O_4$ and γ-Al_2O_3 are the most common on high surface area spinels (40 to 70 m^2/g). This suggests that a careful analysis of the octahedral cation arrangements should be done for those planes.

For the (110) plane, linear chains are interconnected by a tetrahedral cation located in this plane, and an octahedral cation in the sublayer, as represented in Scheme 4. For any given position of a cuprous ion in an octahedral environment, the minimum arrangement describing the geometry of the site corresponds to the section highlighted by the dotted line in Scheme 4. It appears that four oxygen atoms, that can be removed to form anionic vacancies, are shared between the central cuprous ion and another octahedral cation located in the plane or in the sublayer. Therefore, a C or CH structure (α) for the (110) plane can be represented by Scheme 5. On the (100) plane, similar linear chains of octahedral

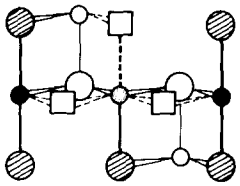

SCHEME 5. Structure of α sites.

cations are observed, but are interconnected by tetrahedral and octahedral cations located in the sublayer (Scheme 6). As for the (110) plane, a linear arrangement of three cations should be considered as highlighted in Scheme 6. However, five oxygens can be removed to form a vacancy on the surface. One of these, located in the overlayer, is only bounded to the cuprous ion and will probably always be removed because of its lower stability. Among the four other oxygens located in the plane, two are shared between the central atom and another octahedral cation, and two are shared with the Cu(I) ion and two octahedral cations. Consequently, three different C and CH structures (β) can be obtained and are described in Scheme 7. Finally, in the (111) plane, a bidimensional arrangement of octahedral cations is observed as described in Scheme 8. All the oxygens, which form a close-packed system, are located in the overlayer and are shared by either two or three cations as shown by the minimum arrangement highlighted in Scheme 8. The corresponding C and CH structures (γ) are described in Scheme 9.

For the copper–chromium systems, and the copper aluminate, the relative concentration of copper ions (Cu(I) or Cu(II)) in octahedral sites is always lower than 0.25. Therefore, one should expect that most of the anionic vacancies associated to the central cuprous ion will be shared between the Cu(I) and the Cr(III) or Al(III) ions. The probability for the existence of those bimetallic shared vacancies (BMV) can be estimated by considering a simple statistical distribution of copper and M(III) cations around the central Cu(I) atom (see Appendix). The probabilities for the various structures (α_i, β_i, and γ_i) corresponding to the (110), (100), and (111) planes are compiled in Table 11 for the catalysts we have studied. In this table, i represents the number of BMV involved in the catalytic sites. Note that for any catalyst, the probability of having one BMV per site is higher than 97.5% and higher than 72.7% for two BMV. In addition, at least 44% of the C sites in the (100) and (111) planes will be constituted only of BMV. It is important to note that these probabilities are almost independent of the crystallographic plane. Consequently, the crystal size and shape will have very little influence on the catalytic properties with the exception of surface areas.

The hydride ions involved in the hydrogenation reaction are likely to be located in a BMV, rather than in a vacancy associated to a single cuprous ion. Therefore, these

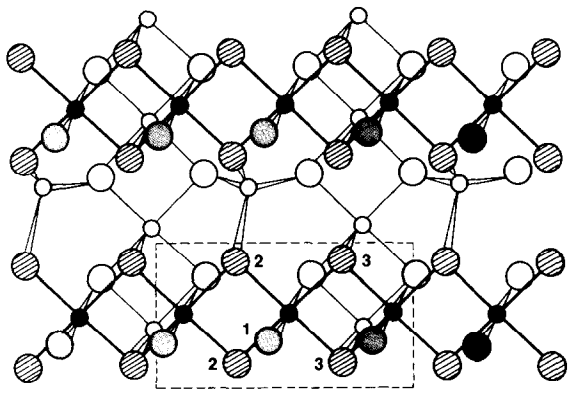

SCHEME 6. Environment of octahedral cations in the (100) plane.

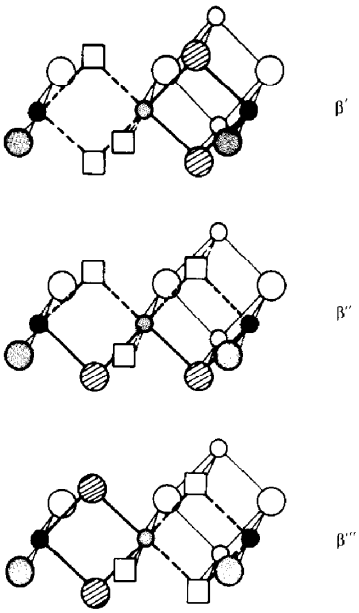

○ Cations : Black = M^{3+} or Cu in the Plane, Gray = Cu^{+} in the Plane
White = M^{3+} or Cu in the Sublayer

◯ Anions : Gray in the Overlayer, Stripped in the Plane, White in the Sublayer

□ Vacancy

SCHEME 7. Structures of β sites.

hydrides are shared between the cuprous ion and the Cr(III) or Al(III) ions. The CH structures are derived from the C structures α, β, γ represented in Schemes 5, 7, and 9 by replacing one of the BMV with a hydride ion. Such structures are consistent with the synergism generally reported for Cu–Cr and Cu–Al mixed oxides as well as with the

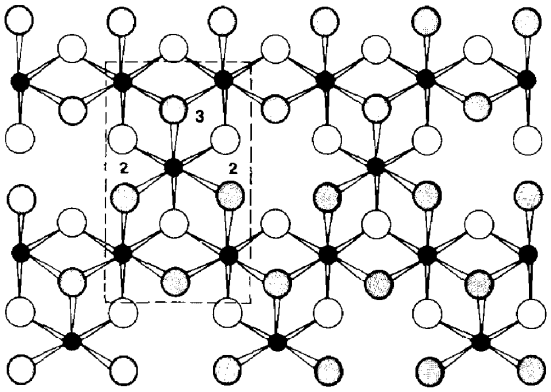

○ Cations : Black in the Plane,

◯ Anions : Gray in the Overlayer, White in the Sublayer

SCHEME 8. Environment of octahedral cations in the (111) plane.

TABLE 11

Sites	Concentration	CuCr-0.5* $x^a = 0.05$	CuCr-0.5 $x = 0.075$	CuCr-1 $x = 0.24$	CuAl-0.5 $x = 0.20$
α_3	$(1 - x)^3$	0.857	0.791	0.439	0.512
α_2	$3x(1 - x)^2$	0.135	0.193	0.416	0.384
α_1	$3x^2(1 - x)$	0.007	0.016	0.131	0.096
α_0	x^3	<0.001	<0.001	0.014	0.008
β_2	$\frac{1}{3}[(1 - x)^2(x^2 + 3x + 3)]$	0.948	0.921	0.727	0.777
β_1	$\frac{1}{3}[x(1 - x)(2x^2 + 4x + 3)]$	0.051	0.077	0.248	0.207
β_0	$\frac{1}{3}[x^2 + x^3 + x^4]$	<0.001	0.002	0.025	0.017
γ_3	$(1 - x)^3(1 + x)$	0.900	0.851	0.544	0.614
γ_2	$x(1 - x)^2(3x + 2)$	0.097	0.143	0.377	0.333
γ_1	$x^2(1 - x)(1 + 3x)$	0.003	0.006	0.075	0.051
γ_0	x^4	<0.001	<0.001	0.003	0.002

[a] x = relative concentration of copper atoms in octahedral sites.

support effect observed on alumina-supported catalysts (*20, 37*). In addition, one can speculate that similar conclusions will be obtained with any copper catalyst in which the second cation is known to form a bond with hydridic species. Since the Cu(I) species are reported by numerous authors as the active species in the methanol synthesis, the existence of these cuprous hydride species is likely to occur in the copper–zinc system because of the well-known formation of Zn^{2+}, H^- pairs in reduced zinc oxides. Further support can be found in two recent studies where the activity of copper chromites for the methanol synthesis correlates with the Cu(I) concentration (*26*), and where the Cu–Zn–O exhibits some hydrogen storage properties (*38*).

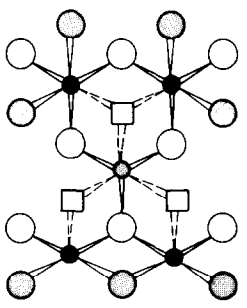

SCHEME 9. Structure of γ sites.

CONCLUSION

An analysis of various copper-based catalysts demonstrates the critical importance of cuprous ions in an octahedral environment for the hydrogenation. Tetrahedral cupric cations are generally unstable and are reduced to metallic copper. Cuprous ions in a linear-like environment (Cu_2O or $Cu(I)CrO_2$) are totally inactive. In addition, the amount of occluded hydrogen, which depends upon the synthesis temperature, is associated with the disorder of the solid, and the ability of the Cr(III) and Al(III) cations to stabilize a defect spinel framework. The second cation is also involved in the structure of the catalytic site, by sharing hydride species and anionic vacancies (BMV) with the cuprous ion. In view of the spinel unit cell, new structures of the catalytic site are proposed for the most common crystallographic planes. The probability of BMV is high for all of these structures and is almost independent of the crystal shape and size. Finally, these structures explain the well-known synergism between chromium or aluminum and copper.

APPENDIX

The various structures of the catalytic sites in one given crystallographic plane can be described by the number of vacancies shared by the central cuprous ion and the chromium or aluminum ions (BMV). For the (110), all the possible vacancies are shared by two octahedral cations. The distribution of the various structures α_i, where i is the number of BMV, follows a binomial distribution (Scheme 5):

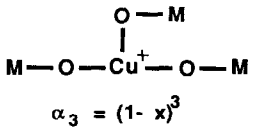

$\alpha_3 = (1- x)^3$

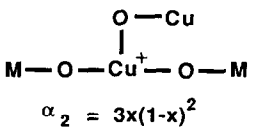

$\alpha_2 = 3x(1-x)^2$

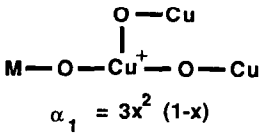

$\alpha_1 = 3x^2 (1-x)$

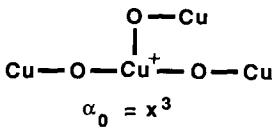

$\alpha_0 = x^3$

where x and $(1 - x)$ are the relative concentrations of the copper ions (Cu(I) + Cu(II)) and the chromium or aluminum ions in octahedral sites.

In the β and γ structures, some possible vacancies are shared by three cations. Therefore, the probability of having at least one chromium or aluminum involved is $(1 - x^2)$ instead of $(1 - x)$ for a BMV.

For the γ sites, the distribution is (Scheme 9)

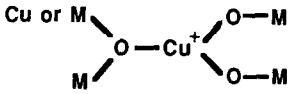

$\gamma_3 = (1-x^2)(1-x)^2$

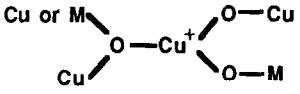

$\gamma_2'' = 2x(1-x)(1-x^2)$

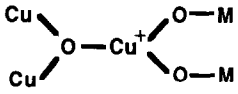

$\gamma_2' = x^2 (1-x)^2$ $\quad \gamma_2 = x(1-x)^2 (3x+2)$

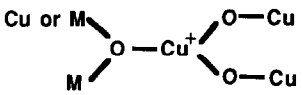

$\gamma_1' = x^2 (1-x^2)$

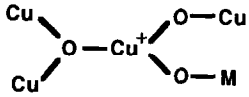

$\gamma_1'' = 2x^3 (1-x)$ $\quad \gamma_1 = x^2 (1-x)(1+3x)$

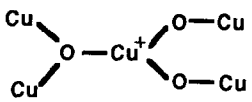

$\gamma_0 = x^4$

For the β structures, one vacancy will not be shared at all, and two vacancies must be chosen out of four oxygen atoms. Among these four possible vacancies, two are shared by two cations and the two others are shared by three cations. Therefore, three different structures are possible and correspond to the β', β'', β''' structures represented in Scheme 7. For simplicity, we assumed that these three structures have the same probability of existence, and an average distribution was calculated, according to the preceding section:

$$\beta_2 = \tfrac{1}{3}[(1 - x)^2(x^2 + 3x + 3)]$$

$$\beta_1 = \tfrac{1}{3}[x(1 - x)(2x^2 + 4x + 3)]$$

$$\beta_0 = \tfrac{1}{3}[x^2 + x^3 + x^4].$$

ACKNOWLEDGMENTS

We thank J. L. Gland for helpful comments and discussions.

REFERENCES

1. Mounts, T. L., and Dutton, H. J., *J. Amer. Oil Chem. Soc.* **44,** 67 (1967).
2. Koritala, S., Selke, E., and Dutton, H. J., *J. Amer. Oil Chem. Soc.* **50,** 310 (1973).
3. Koritala, S., *J. Amer. Oil Chem. Soc.* **47,** 463 (1970).
4. Isagulyants, V. I., *Izd. Akad. Nank Armen SSR Yerevan* (1947).
5. Dorsky, J., Tavares, R. F., Easter, W. R., and Brit. Patent No. 1.340.409 (1973).
6. Sokol'skii, D. V., Pak, A. M., and Ginzburg, M. A., *React. Kinet. Catal. Lett.* **18,** 311 (1979).
7. Klier, K., "Advances in Catalysis" (D. D. Eley, P. W. Selwood, P. B. Weisz, Eds.), Vol. 31, p. 243. Academic Pres, New York, 1982.
8. Apai, G., Monnier, J. R., and Hanrahan, M. J., *J. Chem. Soc. Chem. Commun.* **212,** (1984).
9. Bechara, R., Wrobel, G., Daage, M., and Bonnelle, J. P., *Appl. Catal.* **16,** 15 (1985).
10. Daage, M., and Bonnelle, J. P., "Proceedings of the International Symposium, Lyon" (G. M. Pajonk, S. J. Teichner, and J. E. Germain, Eds.), p. 261. Elsevier, Amsterdam, 1983.
11. Daage, M., and Bonnelle, J. P., *Appl. Catal.* **16,** 335 (1985).
12. Weller, S., and Mills, G. A., *J. Amer. Chem. Soc.* **75,** 769 (1953).
13. Wrobel, G., Walter, P., and Beaufils, J. P., *C.R. Acad. Sci. C* **283,** 335 (1976).
14. Wrobel, G., Arsene, J., Lenglet, M., D'Huysser, A., and Bonnelle, J. P., *Mater. Chém.* **6,** 19 (1981).
15. Garin, F., and Gault, F. G., *J. Amer. Chem. Soc.* **97,** 4466 (1975).
16. Gault, F. G., and Kemball, C., *Trans. Faraday Soc.* **57,** 1781 (1961).
17. Mintsa-Eya, V., Thesis, Strabourg, France, 1977.
18. Nishimura, E., Inoue, Y., and Yasumori, I., *Bull. Chem. Soc. Japan* **48,** 803 (1975).
19. Stroupe, J. D., *J. Amer. Chem. Soc.* **71,** 569 (1949).
20. Okkerse, C., Dejonge, A., Coenen, J. W. E., and Rozendahl, A., *J. Amer. Oil Chem. Soc.* **44,** 152 (1967).
21. Taghavi, M. B., Pajonk, G. M., Teichner, S. J., *J. Colloid Interface Sci.* **71,** 451 (1979).
22. Aissi, C. F., Daage, M., Guelton, M., Bonnelle, J. P., B'Nagy, J., and Derouane, E. G., *J. Catal.* **76,** 231 (1982).
23. Jalowiecki, L., Daage, M., Bonnelle, J. P., and Tchen, A. H., *Appl. Catal.* **16,** 1 (1985).
24. D'Huysser, A., Wrobel, G., and Bonnelle, J. P., *Nouv. J. Chim.* **6,** 437 (1982).
25. Adkins, H., Burgoyne, E. E., and Schneider, H. J., *J. Amer. Chem. Soc.* **72,** 2626 (1950).
26. Bechara, R., Thesis, Lille, France, 1986.
27. Codey, R. F., and Reed, S., *J. Amer. Ceram. Soc.* **55,** 395 (1972).
28. Wrobel, G., D'Huysser, A., and Bonnelle, J. P., *Nouv. J. Chim.* **8,** 291 (1984).
29. Selwood, P. W., *J. Amer. Chem. Soc.* **92,** 39 (1970).
30. Siegel, S., *J. Catal.* **30,** 139 (1973).
31. v.d. Berg, J., v. Dillen, A. J., v.d. Meijden, J., and Geus, J. W., *NATO Adv. Study Inst. Ser. Ser. C* **105,** 493 (1982).
32. v.d. Meijden, J., Thesis, Utrecht, Netherlands, 1981.
33. Wells, A. J., "Structural Inorganic Chemistry," 4th ed., p. 220. Oxford Univ. Press (Clarendon), Oxford, 1975.
34. "Handbook of Chemistry and Physics," 65th ed., Vol. F, p. 165 1985.
35. Beaufils, J. P., and Barbaux, Y., *J. Appl. Crystallogr.* **15,** 301 (1982).
36. Beaufils, J. P., and Barbaux, Y., *J. Chim. Phys.* **78,** 347 (1981).
37. Ipatieff, V. N., Corson, B. B., and Kurbatov, J. D., *J. Phys. Chem.* **44,** 670 (1960).
38. Wrobel, G., Bali, F., Jalowiecki, L., Bonnelle, J. P., submitted for publication.